^{1}H and ^{31}P NMR and EPR of Pentaammineruthenium(III) Complexes of Endocyclically Coordinated Nucleotides, Nucleosides, and Related Heterocyclic Bases. Autoxidation of [(Guoκ^{N7})$(NH_3)_5Ru^{III}$] (Guo = Guanosine). Crystal Structure of [7MeGua$\kappa^{N9}$$(NH_3)_5$Ru]$Cl_3\cdot 3H_2O$

V. M. Rodriguez-Bailey, K. J. LaChance-Galang,† P. E. Doan,‡ and M. J. Clarke*

Merkert Chemistry Center, Boston College, Chestnut Hill, Massachusetts 02167, and Department of Chemistry, Northwestern University, Evanston, Illinois 60208

Received August 5, 1996[⊗]

The ^{1}H-NMR spectra of complexes involving the paramagnetic metal center [$(NH_3)_5Ru^{III}$] coordinated at ring nitrogens have been examined with pyridine, purine, nucleoside, and nucleotide ligands along with ^{31}P-NMR of the nucleotide complexes and EPR of representative complexes. Variations in the spectra have been investigated as a function of the coordination site and pH. Pseudocontact and contact shifts have been calculated for various protons, and an attempt has been made to correlate sugar conformations in coordinated 5′GMP, 5′IMP, Guo, and Ino with paramagnetically induced shifts. The compound [(7MeGuaκ^{N9})$(NH_3)_5$Ru]$Cl_3\cdot 3H_2O$ crystallizes in the orthorhombic space group $Pna2_1$ with cell parameters $a = 25.375(4)$ Å, $b = 11.803(4)$ Å, $c = 6.958(2)$ Å, $Z = 4$, and $R = 0.042$. The autoxidation of [L$(NH_3)_5Ru^{III}$], where L = Guo, dGuo, and 1MeGuo, to the corresponding 8-oxo complexes under atmospheric oxygen is first order in the complex and [OH^-]. For L = Guo, $k = 6.6 \times 10^{-5}$ M^{-1} s^{-1}, $\Delta H^* = 58$ kJ/mol, and $\Delta S^* = -124$ J/(mol K).

Introduction

Ruthenium complexes have shown promise in the development of several types of anticancer pharmaceuticals, including the following: (1) chemotherapeutic drugs,[1−3] (2) radiosensitizing agents to increase the effectiveness of radiotherapy,[4] and (3) radioscintigraphic complexes for diagnostic imaging.[5,6] In the first two categories, these agents appear to bind directly to nucleic acids to introduce damage that affects replication and translation. A possible consequence of covalent binding is oxidation of a DNA base, and a mechanism for facilitating nucleoside autoxidation following Ru^{III} coordination has been presented.[7]

While covalent binding to DNA generally proceeds much more rapidly with complexes of Ru^{II},[8] coordination to nucleic acids can also occur with Ru^{III} and, probably, Ru^{IV} ions.[9] Moreover, the $E°$ values of $Ru^{III,II}$ couples are often in a range that electron transfer in either direction can occur at biologically available potentials. Consequently, it is necessary to know the effects of both Ru^{II} and Ru^{III} on the conformation of nucleosides, nucleotides, and nucleic acids. NMR techniques provide a convenient means of studying these interactions and are more easily performed on ruthenium(III) complexes, which are more stable with respect to both air oxidation and ligand substitution.

The paramagnetic nature of the low-spin, d^5 Ru^{III} ion strongly affects the NMR spectra of its coordinated ligands.[10,11] In this study, we report on the effects of coordinated [$(NH_3)_5Ru^{III}$] on peak position and line broadening in the ^{1}H NMR spectra of important nucleotides, nucleosides, and their constituent bases and the ^{31}P NMR of 5′GMP and 5′IMP. With appropriate caution, the paramagnetic effects generated by the metal center can be used to assist in assigning the geometry of the complex. Structural data for the compound [7MeGua$(NH_3)_5$Ru]$Cl_3\cdot 3H_2O$ and EPR on representative complexes are also presented.

Procept, Inc., has recently discovered that simple, substitution-inert complexes of Ru^{III} with nitrogen ligands (NH_3, imidazole, pyridine) can be potent immunosuppressants.[12] For example, nanomolar concentrations of [4Mepy$(NH_3)_5Ru^{III}$] (PRO-2844) and *cis*-[$(Im)_2(NH_3)_4Ru^{III}$] (PRO-2846) strongly inhibit T lymphocyte proliferation with few or no acute toxic side effects. Since these ruthenium drugs are mechanistically distinct from present clinically used agents, cyclosporin A and FK506, and may function through an electron-transfer pathway,[11] they point the way toward an exciting new class of immunosuppressive drugs.[12] The NMR and EPR parameters of several series of ammineruthenium(III) complexes of imidazole ligands have been previously reported.[10,11] Herein we report on the ^{1}H NMR

* To whom correspondence should be addressed at Boston College.
† Presently at Regis College, Weston, MA.
‡ Northwestern University.
⊗ Abstract published in *Advance ACS Abstracts,* April 1, 1997.

(1) Clarke, M. J.; Galang, R. G.; Rodriguez, V. M.; Kumar, R.; Pell, S.; Bryan, D. M. In *Proceedings of the 5th International Symposium on Platinum Compounds in Cancer Chemotherpy*; Nicolini, M., Ed.; Kluwer Publishing: Boston, MA, 1987; pp 582−600.
(2) Clarke, M. J. *Prog. Clin. Biochem. Med.* **1989**, *10*, 25−39.
(3) Clarke, M. J. In *Metal Complexes in Cancer Chemotherapy*; Keppler, B. K., Ed.; VCH: Weinheim, Germany, 1993; pp 129−157.
(4) Chan, P. K. Ph.D. Thesis, University of British Columbia, Vancouver, BC, Canada, 1989.
(5) Schachner, E. R.; Gil, M. C.; Som, P.; Oster, Z. H.; Atkins, H. L.; Subramanian, G.; Badia, J.; Srivastava, S. C.; Richards, P.; Treves, S. *J. Nucl. Med.* **1981**, *22*, 352.
(6) Schachner, E. R.; Gil, M. C.; Som, P.; Oster, Z. H.; Atkins, H. L.; Subramanian, G.; Badia, J.; Srivastava, S. C.; Richards, P.; Treves, S. *Nucl. Med. Commun.* **1983**, *4*, 94.
(7) Gariepy, K. C.; Curtin, M. A.; Clarke, M. J. *J. Am. Chem. Soc.* **1989**, *111*, 4947−52.
(8) Clarke, M. J.; Jansen, B.; Marx, K. A.; Kruger, R. *Inorg. Chim. Acta* **1986**, *124*, 13−28.
(9) Rubin, J. R.; Sabat, M.; Sundarlingam, M. *Nucl. Acid Res.* **1983**, *11*, 6571.
(10) LaChance-Galang, K. J.; Doan, P. E.; Clarke, M. J.; Rao, U.; Yamano, A.; Hoffman, B. *J. Am. Chem. Soc.* **1995**, *117*, 3529−3538.
(11) Clarke, M.; Bailey, V. M.; Doan, P.; Hiller, C.; LaChance-Galang, K. J.; Daghlian, H.; Mandal, S.; Bastos, C.; Lang, D. *Inorg. Chem.* **1996**, *35*, 4896−4903.
(12) Bastos, C. M.; OCain, T. D.; Gordon, K. A.; Sampo, T. M.; Clarke, M. J.; Daghlian, H. In *Abstracts of Papers;* 211th National Meeting of the American Chemical Society, New Orleans, LA, Spring 1996; American Chemical Society: Washington, DC, 1996; pp INOR 582.

S0020-1669(96)00941-X CCC: $14.00

of several complexes of the type $[L(NH_3)_5Ru^{III}]$, where L is a pyridine ligand.

Since coordination to ammineruthenium(III) centers facilitates the autoxidation of nucleosides to their 8-oxo derivatives in basic solutions[7] and some ruthenium complexes may enable autoxidation of guanine residues in nucleic acids, the kinetics of $[L(NH_3)_5Ru^{III}]$, where L is a guanine nucleoside, have been measured and compared with those for L = inosine.

Abbreviations: Py, pyridine; 3,5-Lut, 3,5-dimethylpyridine (lutidine); 4-Pic, 4-methylpyridine (picoline); Im, imidazole; Gua, guanine; 7MeGua, 7-methylguanine; 9MeGua, 9-methylguanine; 1,7Me_2Gua, 1,7-dimethylguanine; 2Me_2Gua, N_2,N_2-dimethylguanine; Guo, guanosine; dG; deoxyguanosine; 8-OGuo; 8-oxoguanosine; 8-O-1MeGuo, 1-methyl-8-oxoguanosine. Hyp, hypoxanthine; 7MeHyp, 7-methylhypoxanthine; Ino, inosine; 5′IMP; 5′-inosine monophosphate; 8-OIno, 8-oxoinosine; 8-O-Hyp, 8-oxohypoxanthine. Superscript charges on ligands are used to indicate deprotonated ligands, and deprotonation sites are indicated in the tables or in the text where these ionized species are discussed. Other abbreviations: TSP, 3-(trimethylsilyl)propionic acid; TMP, trimethyl phosphate.

Experimental Section

Materials and Synthesis. Ligands were obtained from Aldrich or Sigma and used without further purification. In general, the pentaammineruthenium(III) complexes of the various ligands were prepared by direct combination with $[(H_2O)(NH_3)_5Ru]^{2+}$ followed by air oxidation.[13−17] Purities of all complexes were verified by HPLC on a C_{18} column with 10% methanol in 0.5 M ammonium propionate as the eluent. For nucleotidyl complexes, purity was most conveniently determined by ^{31}P NMR. Synthetic references to compounds previously reported are given in Table 3. $[(NH_3)Ru^{III}]_n$−DNA was prepared by previously reported methods.[8,18]

[7MeGuaκ^{N9}(NH$_3$)$_5$Ru]Cl$_3$ was synthesized by reducing $[H_2O(NH_3)_5Ru](CF_3CO_2)_2$ with a 10% excess of ligand at pH 12 over zinc amalgam under an argon atmosphere for 45 min. After removing the Zn, adjusting to pH 4, and oxidizing by air bubbling for 1 h, the resulting purple solution was chromatographed on Dowex-50W-X2. The desired purple band was eluted with 3 M HCl and vacuum evaporated to dryness. The residue was dissolved in a minimum of 0.1 M HCl, and absolute ethanol was allowed to diffuse into the solution yielding purple crystals. Yield: 75%. Anal. Calcd for $[Ru(NH_3)_5(7MeGua)]Cl_3\cdot 3H_2O$: C, 14.08; H, 5.52; N, 27.37; Cl, 20.78. Found: C, 14.25; H, 5.25; N, 27.00; Cl, 20.47. UV−vis, λ_{max} (nm): 284, 325, 555. pK_a (UV−vis): 7.84 ± 0.06. $E° = 130$ mV.

[8-OGuoκ^{N7}(NH$_3$)$_5$Ru]Cl$_2$ was prepared by analogy to the synthesis of $[8\text{-OIno}(NH_3)_5Ru]Cl_2$.[7] A solution of $[Guo(NH_3)_5Ru]Cl_3$ was adjusted to pH 10 and oxidized with oxygen for about 12 h. The resulting blue solution was chromatographed on a Biorex-70 column from which the desired band eluted with 0.6 M ammonium formate. The buffer was removed by placing the sample on a Dowex-50 X2 column and eluting with several bed volumes of water. The complex was then removed with 3 M HCl, the volume was reduced to a minimum by rotary vacuum evaporation, and absolute ethanol was added to induce precipitation. The blue compound was collected by filtration and dried in a vacuum desiccator. Anal. Calcd for $[8\text{-OGuo}(NH_3)_5Ru]Cl_2\cdot 2.5H_2O$: C, 20.00; H, 5.38; N, 23.33. Found: C, 20.19; H, 4.95; N, 23.15. UV-vis, λ_{max} (nm): 249, 290, 370 (sh), 682.

[8-O-1MeGuoκ^{N7}(NH$_3$)$_5$Ru]Cl$_2$ was similarly synthesized from $[1MeGuo(NH_3)_5Ru]Cl_3$. Anal. Calcd for $[8\text{-O-1MeGuo}(NH_3)_5Ru]Cl_2\cdot 2H_2O$: C, 21.82; H, 5.50; N, 23.14. Found: C, 21.87; H, 5.17; N, 22.95. UV−vis, λ_{max} (nm): 255, 284, 370 (sh), 680.

NMR. For routine spectra, 10 mg samples were lyophilized three times in 99.8% D_2O (Aldrich) to minimize the proton concentration and then dissolved in 0.6 mL of 100% D_2O ([Ru] = ∼40−50 mM). Both one-dimensional and COSY spectra were recorded on a Varian XL-300 NMR spectrometer using 5 mm oven-dried NMR tubes at 18.8 °C. A 100 ppm (50 to −50 ppm) spectral width and a 5.00 Hz bandwidth were normally employed in obtaining one-dimensional ^{1}H spectra. The intense HOD solvent resonance was suppressed by the WEFT technique.[19,20] Proton chemical shifts were measured relative to TSP. The effects of intermolecular paramagnetic interactions were tested for by measuring the spectrum of representative complexes as a function of concentration from 20 to 220 mM. Concentration effects were usually less than ∼0.2 ppm and were always considerably smaller than the intramolecular effects of the paramagnetic ion.

^{31}P NMR were recorded using the same probe and samples similarly constituted. δ-values are reported relative to trimethyl phosphate. For nucleotide and DNA complexes, the average number of transients/sample collected was 200 and 5000, respectively. ^{1}H NMR were taken immediately prior to the ^{31}P spectra to ensure sample purity. For nucleotide complexes, the sweep width was 60 ppm with phosphoric acid as an external standard. For DNA complexes, the sweep width was 80 ppm (40 to −40 ppm) with a 5.00 Hz bandwidth and TMP as the internal standard.

T_1 measurements were generally made using the inversion recovery method; however, when paramagnetic line widths were large, the relationships $T_1 = T_2 = 1/\pi\Delta\nu_{1/2}$ were used to estimate the relaxation time.[21] In order to eliminate the paramagnetic effects of dissolved oxygen, samples were purged with argon or subjected to freeze−thaw cycles under vacuum.

pH was adjusted with small amounts of DCl and NaOD (Aldrich) and the pH measured before and after each run with a combination glass microelectrode (Ingold Inc.). After standardizing in pH 4 and 7 buffers, the pH electrode was soaked in D_2O prior to use. The pH reading was not corrected for the isotope effect. pK_a values were derived from a least-squares fit of chemical shift versus pH.

Dispersion-mode EPR spectra were collected under rapid-passage conditions at 2 K with both X-band (9.5 GHz)[10] and Q-band (35 GHz) spectrometers, which have been described previously[22,23] along with the advantages of using adiabatic rapid-passage conditions for broad EPR signals.[24] Compounds were dissolved (1−2 mg/mL) in a 2:1 (v:v) water/ethylene glycol mixture with the pH adjusted to pH 5−6. A copper background signal that originated in the cavity was digitally subtracted from all X-band spectra. Because the magnets have a limit of 1.5 T, only g values greater than 1.7 could be obtained at Q-band.

Since the signal from the lowest g-value was not accessible, it was calculated by using the appropriate g-matrix for a t_{2g}^5 system and performing a least-squares fit to the two observable g-values by varying Δ and V, the tetragonal and rhombic ligand field distortion parameters, respectively.[10,11] As g-values vary little with alkyl substituents, the g-values for some selected complexes were used to estimate values of δ_{dip} in analogous ones.

Crystal Structure Determination. Pertinent crystal data for $[7MeGua(NH_3)_5Ru]Cl_3\cdot 3H_2O$ are given in Tables 1 and S1 (Supporting Information) and crystallographic coordinates for the non-hydrogen atoms are listed in Table S2. Single crystals of $[7MeGua(NH_3)_5Ru]Cl_3\cdot H_2O$ were grown by slow vapor diffusion of ethanol into an aqueous solution of the compound. A suitable crystal was mounted on a glass fiber, which was placed in the beam of a Rigaku AFC5R diffractometer. Space group assignment was based on the systematic absences of 0kl,

(13) Clarke, M. J.; Taube, H. *J. Am. Chem. Soc.* **1974**, *96*, 5413−5419.
(14) Clarke, M. J.; Taube, H. *J. Am. Chem. Soc.* **1975**, *97*, 1397−1403.
(15) Clarke, M. J. *Inorg. Chem.* **1977**, *16*, 738−744.
(16) Ford, P.; Rudd, d. F. P.; Gaunder, R.; Taube, H. *J. Am. Chem. Soc.* **1968**, *90*, 1187−94.
(17) Sundberg, R. J.; Bryan, R. F.; Taylor, I. F.; Taube, H. *J. Am. Chem. Soc.* **1974**, *96*, 381−92.
(18) McNamara, M.; Clarke, M. J. *Inorg. Chim. Acta* **1992**, *195*, 175−185.
(19) Patt, S. L.; Sykes, B. D. *J. Chem. Phy.* **1975**, *56*, 3182.
(20) Redfield, A. G.; Kunz, S. D.; Ralph, E. K. *J. Magn. Reson.* **1975**, *19*, 114.
(21) Drago, R. S. In *Physical Methods in Chemistry*; W. B. Saunders: Philadelphia, PA, 1977.
(22) Cline, J.; Reinhammar, B.; Jensen, P.; Venters, R. A.; Hoffman, B. M. *J. Biol. Chem.* **1983**, *258*, 5124.
(23) Werst, M. M.; Davoust, C. E.; Hoffman, B. M. *J. Am. Chem. Soc.* **1991**, *113*, 1533−1537.
(24) Mailer, C.; Taylor, C. P. S. *Biochim. Biophys. Acta* **1973**, *322*, 195−203.

Table 1. Crystallographic Data for $[(7MeGua\kappa^{N9})(NH_3)_5Ru]Cl_3 \cdot 3H_2O$

formula	$H_{28}C_6N_{10}O_4Cl_3Ru$
fw	511.78
space group, crystal system	*Pna*2$_1$ (No. 33), orthorhombic
color	purple
cryst dimens (mm)	0.1 × 0.1 × 0.1
cell constants	$a = 25.375(4)$ $b = 11.803(4)$ $c = 6.958(2)$
cell vol (Å^3)	2084(1)
Z (fw/unit cell)	4
μ (cm^{-1}), rel transm factors	11.56, 0.86−1.0
temp (°C)	23
radiation source, λ (Å)	Mo Kα, 0.710 69
scan mode	$\omega-2\theta$
$2\theta_{max}$ (deg)	55.1
d_{calcd} (g/cm^3)	1.631
tot. no. of unique observns	2783
obsd reflcns[a]	1858
no. of variables in least squares	216
$R = \sum(\|F_o\| - \|F_c\|)/\sum\|F_o\|$	0.042
R_w[b] $= [\sum w((F_o\| - \|F_c\|)^2/\sum w(F_o)^2\|]^{1/2}$	0.051
goodness of fit $= [\sum w(\|F_o\| - \|F_c\|)^2/(N_{obs} - N_{params})]^{1/2}$	1.52

[a] $T = 20(1)$ °C. Reflections with $F_o > 3\sigma(F_o)$ were retained as observed and used in the solution and refinement of the structure. Three standard reflections were monitored with a limit of 0.2% variation. Function minimized: $\sum w(|F_o| - |F_c|)^2$. [b] Weighting scheme: $w = 4(F_o)^2[\sigma^2/(F_o)^2]^2$.

$k + 1 \neq 2n$, and $hk0$, $h \neq 2n$. Intensities of three representative reflections, which were measured after every 150 reflections, remained constant throughout data collection. The Ru atom was located by direct methods, and the structure was solved from difference Fourier maps.[25,26] The non-hydrogen atoms were refined anisotropically. Hydrogen atoms on the purine ring were located from difference maps while the ammine protons were included in the structure factor calculation in idealized positions (C−H = 0.95 Å, N−H = 0.87 Å). All hydrogens were assigned isotropic thermal parameters, which were 20% greater than the B_{equiv} value of the atom to which they were bonded. Refinement was by full-matrix least squares. Neutral atom scattering factor and anomalous dispersion effects were included in F_c; the values for $\Delta f'$ and $\Delta f''$ were those of Cromer.[27]

Calculations of Paramagnetic Effects. The QUEST program[28] was used to extract a number of representative crystal structures of monomeric 5′GMP, Guo, 5′IMP, and Ino species from the Cambridge Structural Database. The molecular fragment $[(NH_3)_6Ru]^{3+}$ was then positioned in these models as it appears in the crystal structure of $[(9MeHyp\kappa^{N7})(NH_3)_5Ru^{III}]$[29] by using PCMODEL, Chem-3D, or CACHe molecular editing programs.[30−32] Structural parameters obtained from minimizing a representative example, $[(9MeHyp\kappa^{N7})(NH_3)_5Ru^{III}]$, were found to be in good agreement with X-ray data except for the Ru−N7 bond distance, which was subsequently held to 2.09 Å.[29] Some model nucleoside complexes with *anti*,*2′-endo*,*gg*, *anti*,*3′-endo*,*gg*, and *syn*,*2′-endo*,*gg* conformations constructed from crystallographic data were energy minimized by MM2, in which hydrogen- and π-bonding calculations were included. Reminimizations were usually done to ensure that the structures had reached complete convergence.

The ^{1}H NMR paramagnetic isotropic shifts were calculated as the difference between the observed shift for a given proton in the complex and that for the free ligand ($\delta_{iso} = \delta_{obs} - \delta_{ligand}$). Following the treatment used for a similar series of ammineruthenium(III) complexes with heterocyclic ligands, the pseudocontact shifts resulting from dipolar contributions (δ_{dip}) were estimated from the following equation for $S = {}^1/_2$ at 292 K:[33]

$$\delta_{dip} = \frac{177.79}{r^3}\left\{(3\cos^2(\theta) - 1)\left(g_z^2 - \frac{g_x^2 + g_y^2}{2}\right) + [3/2\ \sin^2(\theta)][\cos(2\phi)](g_y^2 - g_x^2)\right\} \quad (1)$$

Here r (Å) is the Ru−H distance, θ is the angle formed by the Ru−H vector and the Ru−N_{hetero} axis, and ϕ is the angle from the x-axis of the Ru−H vector projected onto the xy-plane.[33] For calculations involving the sugar protons, the term $(2\cos^2(\xi) + \cos^2(\theta) - 1)$, where ξ is the angle x-axis−Ru−H, was substituted for $[\sin^2(\theta)]\cos(2\phi)$. [Note: This relation arises since $\cos(\theta)$ is the projection onto the z-axis and $\cos(\xi)$ is the projection onto the x-axis, so that $1 - \cos^2(\theta) - \cos^2(\xi)$ is the square of the projection onto the y-axis. Consequently, $[\sin^2(\theta)]\cos(2\phi) = x^2 - y^2 = \cos(\xi)^2 - (1 - \cos(\theta)^2 - \cos(\xi)^2 = 2\cos(\xi)^2 + \cos(\theta)^2 - 1$. Use of this relation facilitates the permutation of the axes in attempting to determine the most consistent assignment of the axes.] The ground state in these and similar complexes[10,11] lies at least 1.4 λ below the first excited state configuration, so there is no significant thermal population of the excited state doublets at room temperature; consequently, the NMR results can be interpreted by using the ground-state g values.[10,11,34]

Since crystal structures with planar heterocycles complexed to $[(NH_3)_5Ru^{III}]$ show the heterocycles to be staggered between *cis*-ammines,[10,29,35] ϕ in eq 1 was taken to be 90° ($\cos(2\phi) = -1$) for the heterocyclic ring protons in the pyridine complexes. Values of r, θ, and ϕ (or ξ) were measured from computer-generamed structural models based on crystallographic coordinates.[29,36,37] The contact (through bond) paramagnetic shift was then evaluated as $\delta_{con} = \delta_{iso} - \delta_{dip}$.

As the sugar protons on carbons C2′−C5′ are the least likely to be affected by contact interactions and the contact shift should decrease progressing down this sequence, the product of the correlation coefficients ($-R_dR_c$) between δ_{iso} and δ_{dip} (R_d) and δ_{con} and position in the carbon chain (R_c) was used as an indicator of correlation between possible sugar conformations and the ^{1}H NMR shift patterns as determined from both crystallographic and crystallographic/energy-minimized structures.

Calculated hyperfine coupling constants, A_H (Table S10), for the base ring protons and signs for A_N for the heterocyclic ligand atoms (Figures S1−S4) were obtained from ZINDO[38,39] methods using the CACHe system[32] on computer-generated structural models of $[L(NH_3)_5Ru]^{3+}$, where L = pyridine, imidazole, and purine ring systems. The calculations used the UHF INDO/1 method for the doublet states, which takes into account spin polarization and hyperconjugation effects.[40] As the ZINDO calculations appeared to overestimate A_H values, only the signs and the relative magnitudes are considered here. A test of this method on a previously studied system, $[(Im)(NH_3)_5Ru^{III}]$,[10,11] yielded reasonable quantitative correlations and excellent correlations with regard to sign for both δ_{iso} and δ_{con} versus calculated A_H (see Figures S2 and S3).

(25) Gilmore, C. J. *J. Appl. Crystallogr.* **1984**, *17*, 42−46.
(26) Beurskens, P. T. DIRDIF, Technical Report, 1984, Crystallographic Laboratory, Toernooiveld, Nijmegen, The Netherlands.
(27) Cromer, D. T.; Weber, J. T. *International Tables for X-ray Crystallography*; Kynoch Press: Birmingham, England, 1974; Vol. IV, Tables 2.2 A and 2.3.1.
(28) Allen, F. H.; Bellard, S.; Brice, M. D.; Cartwright, B. A.; Doubleday, A.; Higgs, H.; Hummelink, T.; Hummelink-Peters, B. G.; Kennard, O.; Motherwell, W. D. S.; Rodgers, J. R.; Watson, D. G. *Acta Crystallogr.* **1979**, *B35*, 2331−2339.
(29) Kastner, M. E.; Coffey, K. F.; Clarke, M. J.; Edmonds, S. E.; Eriks, K. *J. Am. Chem. Soc.* **1981**, *103*, 5747−5752.
(30) Gilbert, K. E. PC Model 1.0 ed.; Serena Software: Bloomington, IN, 1988.
(31) Rubenstein, M.; Rubenstein, S. *CHEMDRAW-3D*; 2.0 ed.; Cambridge Scientific Computing, Inc.: Cambridge, MA, 1989.
(32) CACHe Scientific, I: *CACHe*; TekGraphics: Beverton, OR, 1994.
(33) Bertini, I.; Luchinat, C. *NMR of Paramagnetic Molecules in Biological* Systems; Benjamin Cummings: San Francisco, CA, 1986; pp 36−38.
(34) Kurland, R. J.; McGarvey, B. R. *J. Magn. Reson.* **1970**, *2*, 286−301.
(35) Wishart, J. F.; Zhang, X. A.; Isied, S. S.; Potenza, J. A.; Schugar, H. J. *Inorg. Chem.* **1992**, *31*, 3179−3181.
(36) Poojary, M. D.; Manakar, H. J. *J. Chem. Soc., Dalton Trans.* **1988**, 1297−1302.
(37) Martin, R. B. *J. Chem. Educ.* **1987**, *64*, 402.
(38) Bacon, A. D.; Zerner, M. C. *Theor. Chim. Acta* **1979**, *53*, 21−54.
(39) CACHe™, ZINDO, Terra Pacific Writing Corp., Beaverton, OR 97075, 1991.
(40) Sadlej, J. In *Semi-Empirical Methods of Quantum Chemistry*, PWN-Polish Scientific Publishers; John Wiley and Sons: Warsaw, New York, 1985; pp 208−294.

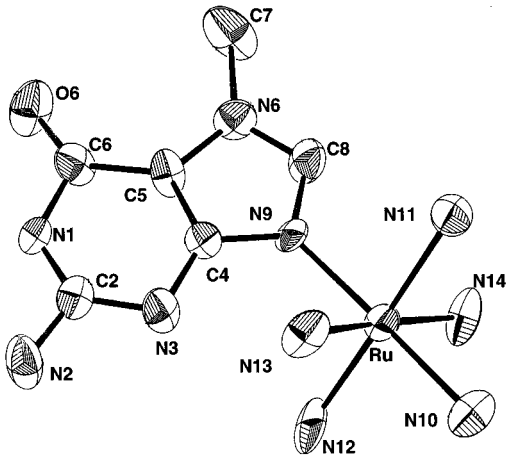

Figure 1. ORTEP diagram of [(7MeGuaκ^{N9})$(NH_3)_5Ru^{III}$].

Table 2. Second-Order Rate Constants and Activation Parameters for the Autoxidation of $[L(NH_3)_5Ru^{III}]$ in Air at 25 °C and $\mu = 0.1$

ligand	k_1 (M^{-1} $s^{-1}/10^{-2}$)	ΔH^* (kJ/mol)	ΔS^* (kJ/(mol K))
dGuo	3.5 ± 0.3		
Guo[a]	6.6 ± 0.3	58 ± 4	-124 ± 19
1MeGuo	20 ± 1		
Ino[b]	77 ± 5	54 ± 4	-120 ± 21

[a] Activation parameters measured at pH 12.00, $\mu = 0.1$. [b] Taken from ref 7. Activation parameters measured at pH 10.27, $\mu = 0.1$.

Kinetics. Reaction rates were measured under atmospheric conditions ($[O_2] = 0.268$ mM, $T = 25$ °C) as a function of pH and temperature in phosphate buffers in which the ionic strength was adjusted to 0.1 M with NaCl. Autoxidation reactions of $[L(NH_3)_5Ru]^{3+}$ were monitored at the λ_{max} for the products: 724 nm for L = Guo, 730 nm for L = dGuo, and 680 nm for L = 1MeGuo. All kinetic data were fitted to first-order kinetics expressions by standard regression methods.

Results

Structure of [(7MeGuaκ^{N9})$(NH_3)_5$Ru]$Cl_3 \cdot 3H_2O$. The structure of $[7MeGua(NH_3)_5Ru]^{3+}$ is illustrated in Figure 1, which shows the metal coordinated at N9. Bond distances and angles are summarized in Supporting Information Tables IV and V. The mean deviation of purine atoms from the plane of the purine ring was 0.0471 Å. The guanine ligand essentially bisects the equatorial Ru−N bonds, with an angle of 43.9° from the plane defined by N9, N10, N11, and N12. The purine rings of adjacent complexes stack such that the pyrimidine ring of one overlays the N1−C6 bond on another at a distance of 3.41 Å. A network of hydrogen bonding exists between the three water molecules, the ammine ligands, and the three chlorides. The water molecule involving O_2 is also hydrogen bonded to the guanine carbonyl (O6) at a distance of 2.88(1) Å.

Kinetics. Autoxidation reactions for $[L(NH_3)_5Ru]^{3+}$ (L = Guo, 1MeGuo, and dGuo) did not occur in the absence of air. In air ($[O_2] = 0.268$ mM), the reactions were first order in both the ruthenium complex and hydroxide. By analogy to the autoxidation reactions for a corresponding series of inosine complexes, these reactions are taken to be approximately first order in $[O_2]$ at atmospheric pressure.[7] Second-order rate constants and activation parameters for the autoxidation reactions are listed in Table 2.

^{1}H NMR. Coordination of the paramagnetic $[(NH_3)_5Ru^{III}]$ molecular fragment to heterocyclic ring nitrogens results in strong shifts and significant line broadening of the ^{1}H NMR ring-proton signals (Table 3). With the exception of H1′, the sugar protons showed relatively small changes in chemical shifts. Nevertheless, line broadening effects generally obscured any proton−proton coupling in the 1D spectra. These effects were generally greater in deprotonated complexes in which an anionic charge resided on the heterocyclic base. Despite the paramagnetic line broadening, it was often possible to observe coupling patterns in the 2D COSY spectra of neutral ligand complexes (Figures S5−S9).

Pyridine Complexes. Peak assignments in the pyridine complexes were made by systematic methylation of the ligands and are consistent with the inverse relationships between the Ru−proton distance (r) and line shifts and line broadening[21,41,42] (cf. Table 3). As in the corresponding imidazole complexes,[10,11] the proximal proton (H2) *ortho* to the metal coordination site exhibits both a dramatic upfield shift and appreciable line broadening relative to free pyridine. The *para*-proton (H4) resonance shows an upfield shift that is somewhat smaller but with a fairly broad line width. The *meta* (H3) resonance is essentially unshifted from free pyridine and has the sharpest line width. Methyl proton peaks are shifted in the opposite direction from those for the ring protons at the same positions. In the case of CH_3(4), these resonances are shifted downfield by somewhat more than the corresponding ring proton peak is shifted upfield. In contrast to the corresponding imidazole complexes,[10,11] methyl substitution does not substantially affect the shifts of the remaining ring protons. The good quantitative correlations and excellent sign correlations between δ_{iso} and δ_{con} and the calculated A_H values for these complexes (see Figures S3 and S5) are consistent with an appropriate choice of magnetic axes and that spin density from the Ru^{III} is delocalized largely through the π system.

Purine Complexes. A comparison of the ^{1}H NMR spectra for the κ^{N7}-bound guanine and hypoxanthine complexes makes the assignments of H2 and H8 resonances unequivocal. In general, the resonance for H2 is broadened and shifted somewhat upfield relative to the free ligand, while that for H8, because of its closer proximity to the metal ion, undergoes a much larger upfield shift and is considerably more broadened. For neutral-ligand complexes with Ru^{III} at N7, H8 appears in the ranges of −26 to −35 ppm for guanine ligands, −14 to −18 for hypoxanthine, and −23 for the xanthine ligand, theophylline. These are all within range of −20 to −40 for H2 for the analogous imidazole complexes.[10,11]

As illustrated in Figure 2, ionization of the purine ring also causes significant shifts in the proton resonances. The H8 resonances in the κ^{N7}-complexes shift an additional 2−4 ppm upfield, when N1 is ionized, and 15−30 ppm upfield, when N9 is ionized. The latter is substantially greater than the shift in H2 of the imidazole complexes (2−12 ppm upfield), when ionized at N1.[10,11] In the κ^{N9}-complexes with 1,7Me_2Gua, 7MeGua, and 7MeHyp,[29] the H8 peak is shifted much less upfield ($\delta_{iso} \sim -11$ and −17 for the Gua and Hyp ligands, respectively), and ionization from the N1 of the 7MeHypκ^{N9} complex moves this resonance back downfield less than 1 ppm. In general, the H8 shifts of the purine-κ^{N7} complexes decrease as the size of the substituent on N9 increases, so that δ_{iso}(H8) follows the order H > CH_3 > ribose = deoxyribose > ribose phosphate. The ΔpK_a's of these complexes relative to the free ligands are dependent on the inverse square of the distance between the ionized proton and the Ru^{III}.[29]

In κ^{N7}-complexes of neutral hypoxanthine, H2 is shifted ~4.0 ppm upfield, relative to the free ligand. When ionized at N9,

(41) *NMR of Paramagnetic Molecules*; La Mar, G. N., Horrocks, W. D., Holm, R. H., Eds.; Academic Press: New York, 1973; pp 667+.
(42) Bertini, I.; Luchinat, C. In *Physical Methods in Chemistry*; 2nd ed.; Drago, R. S., Ed.; W. B. Saunders Co.: Philadelphia, PA, 1992; pp 500−566.

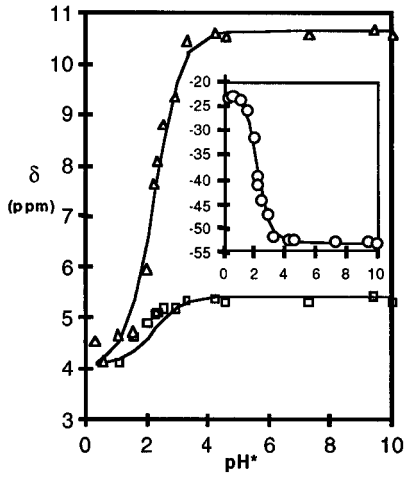

Figure 2. Plot of δ versus pH for the methyl and H8 protons in [(1,3Me$_2$Xanκ^{N7})(NH$_3$)$_5$Ru^{III}]: Δ, CH$_3$(1); [□], CH$_3$(3); ○, H8. Data are fit to the same pK_a* of 2.16 ± 0.03.

this resonance is shifted appreciably further upfield by about 12 ppm; however, when the proton is lost from N1, the resonance shifts back downfield slightly by about 0.5 ppm and is lost under the HOD peak (4.80 ppm). In the complex with 7MeHypκ^{N9}, the H2 resonance is shifted only 0.6 ppm downfield relative to the free ligand and is further shifted an additional 1 ppm downfield on ionization at N1. In 7MeHypκ^{N3}, the relative positions of the H2 and H8 resonances are reversed, since H2 is now adjacent to the metal ion, while H8 is distant. The H8 peak is shifted downfield 3.8 ppm and further downfield with ionization at N9, while the resonance for H2 is shifted considerably upfield (−16.35 ppm) and shifts another ∼4.0 ppm upfield upon ionization from N9.[14] A good correlation exists between the δ_{iso} values and calculated A_H values for the Guaκ^{N9} and Hypκ^{N9} ring systems (see Figures S-7 and S-8 and Table S10), suggesting that π delocalization and contact effects are largely responsible for the paramagnetic shifts of the ring protons in complexes of these ligands. The poor correlation for the 7MeHypκ^{N3} and 7MeHypκ^{N9} complexes appears to be due to relatively small shifts for H2 in the former and the methyl group in the latter, which may be outweighed by dipolar effects. More significantly, the signs of A_H for H8 are incorrect in both complexes, yet the signs expected on the basis of the calculated spin density at C8 in both complexes would yield the correct shift directions (see Figure S4 and Table S10).

Alkyl and Sugar Protons. While not unique, assignments of the methyl substituents in these complexes were made by comparison with similar monomethyl complexes. Assignments of H1′ in κ^{N7}-bound nucleoside complexes were made on the basis of these resonances being strongly shifted in the same direction as for the N9-alkylated complexes, even though, the δ(H1′) values are substantially less upfield than those of the methyl protons (cf., Table 3). The N9 methyl protons on 9MeGuaκ^{N7} and the N3 methyl protons on the analogous 1MeIm complex[11] are shifted downfield by 17−22 ppm relative to the free ligands, while the H1′ sugar resonances are shifted downfield by 8−10 ppm and generally undergo only a ∼1 ppm further downfield shift on ionization at N1. An exception is the δ(H1′) in κ^{N7}-Guoκ^{N7}, which shifts back upfield by 0.6 ppm on N1 ionization. In the region of the pK_a, all peaks are broadened owing to rapid proton exchange at N1. Deprotonation also facilitates gel formation of the various guanine complexes at the relatively high concentrations necessary for NMR studies.

The methyl protons at the 1 and 3 positions of κ^{N7}-1,3Me$_2$-Xanκ^{N7} are only slightly shifted downfield with respect to the free ligand. On ionization at N9, δ(CH$_3$(1)) shifts downfield by an additional 6 ppm, while δ(CH$_3$(3)) shifts only about 1.5 ppm in the same direction.

Assignments of the sugar protons in the nucleoside complexes were made from 2D COSY spectra as shown in Figure S5 for [(Guoκ^{N7})(NH$_3$)$_5$Ru^{III}], which revealed coupling patterns that were obscured by line broadening in the 1D spectra. In the nucleotide complexes, H1′ and H2′ were assigned by their unique downfield and upfield positions, respectively, as well as by coupling evident in the COSY spectra. H3′, H4′, and H5′ were assigned by their COSY coupling with H4′ taken as the peak coupled to both H3′ and H5′. In the nucleoside complexes, δ_{iso}'s for the H2′ through H5′ resonances are in the range −0.7 to 2.5 ppm. In the nucleotide complexes, the resonances for H2′ through H4′ are shifted but remain within this range, while H5′ shows a somewhat larger shift of 2.2 to 3.0 ppm.

The order of the chemical shifts in free guanosine is H1′ > H2′ > H5′ > H4′ > H3′; but in the guanosine and deoxyguanosine complexes, this alters to H1′ > H3′ > H4′ > H5′ > H2′ (H2″). In free inosine the order is H1′ > H2′ > H3′ > H4′ > H5′, which Ru^{III} coordination alters considerably to H1′ > H5′ > H4′ > H3′ > H2′. In the 5′GMP (Figure S8) and 5′IMP complexes, the order varied only slightly from that for Ino; i.e., H1′ > H5′ > H3′ > H4′ > H2′. Comparison of Figures S2 and S3 shows that the pattern of sugar resonances changes considerably between the Guo and 5′GMP complexes, whereas those of Ino and 5′IMP are similar.

8-Oxo Complexes. Autoxidation of many N9-alkylated purines or nucleosides is facilitated by N7-coordination of [(NH$_3$)$_5$Ru^{III}].[7] The resulting 8-oxopurines have an additional acidic hydrogen at N7; however, since this site is already occupied by the metal ion, these ligands are always anionic on the imidazole ring. The H2 resonances in the oxidized hypoxanthine ligands, 8-OHyp and 8-OIno, appear about 30 ppm upfield from the corresponding peaks in the parent complexes. This and the failure of cross peaks to appear in the 2D COSY experiments are probably due to increased spin transfer arising from greater π-donation of electron density from the anionic ligand.

C-Bound Complexes. As with the C2-bound imidazole complexes,[10,11] the ^{1}H NMR spectra of the C8-caffeine complexes are complicated by the kinetic *trans* effect generated by the ylidene ligands[14,17] which causes exchange of the inner-sphere chloride by water. Consequently, these spectra vary with time, chloride concentration, and, especially for the aqua complexes, pH. The pK_a (3.28 ± 0.02) for N9 ionization of *trans*-[Cl(1,3,7Me$_3$Xanκ^{C8})(NH$_3$)$_4$Ru^{III}] as determined by ^{1}H NMR titration is in excellent agreement with that measured spectrophotometrically (3.20 ± 0.05).[14]

In the caffeine complex, the methyl resonances are all shifted downfield relative to the free ligand by varying degrees depending on their distance from the metal ion. Ionization of the *trans*-chloro complex at N9 shifts δ(CH$_3$(7)) an additional 9 ppm downfield, while δ(CH$_3$(3)) moves 2.2 ppm upfield, and the most distant methyl at N1 is relatively unaffected.

Exchange of the chloride for a water leaves δ(CH$_3$(1)) and δ(CH$_3$(3)) relatively unaffected, while δ(CH$_3$(7)) is shifted dramatically downfield. Ionization of the aqua-substituted species (pK_a = 3.25 ± 0.03) occurs in the same region as N9 ionization from the caffeine ligand in the chloro complex. A second pK_a is evident at 8.71 ± 0.03, which is taken to be that for the coordinated water, since δ(CH$_3$(7)) decreases substantially (cf., Table 3). Consequently, the three species are assigned

Table 3. Summary of the ^{1}H NMR Chemical Shifts of [L(NH$_3$)$_5$Ru^{III}] at 18.8 °C in D$_2$O

ligand	coord. site	ion site	proton	δ (ppm)	δ_{dia}[a] (ppm)	δ_{iso} (ppm)	δ_{dip} (ppm)	δ_{con} (ppm)	T_1[b] (ms)	synth ref
pyridine	1		H2	−18.13	8.41	−26.5	4.2	−30.7	1.6	16, 51, 71
			H3	7.51	7.35	0.2	−6.6	6.8		
			H4	−10.97	7.76	−18.7	−7.0	−11.7	9.5	
3,5-Lut	1		H2	−18.03	7.98	−26.0	4.2	−30.2	1.5	
			(CH$_3$)3,5	−3.40	2.13	−5.5	−2.9	−2.6		
			H4	−13.31	7.28	−20.6	−7.0	−13.6		
4-Pic	1		H2	−16.47	8.24	−24.7	4.2	−28.9	1.5	
			H3	9.05	7.61	1.4	−6.6	8.0		
			(CH$_3$)4	25.08	2.26	22.8	−6.5	29.3	5.1	
Gua	7		H8	−34.34	8.66	−43.0	0.7	−43.7	1.41	13
Gua$^-$	7	9	H8	−58.27	7.5	−65.8				
9MeGua	7		H8	−29.72	8.84	−38.6	9.2	−47.7	1.06	13
			CH$_3$(9)	20.99	3.81	17.2	−3.0	20.2	2.15	
9MeGua$^-$	7	1	H8	−33.72	7.61	−41.3			1.52	
			CH3$_(9)$	25.24	3.61	21.6			10.8	
1,7Me$_2$Gua	9		H8	−2.85	8.61	−11.5	−0.4	−11.1	0.66	13
			CH$_3$(1)	7.10	3.43	3.7	−0.3	3.9	80	
			CH$_3$(7)	33.75	4.05	29.7	−6.3	10.0		
7MeGua	9		H8	−2.62	8.48	−11.1			0.97	
			CH$_3$(7)	31.53	3.89	27.6			5.8	
2,2Me$_2$Gua	9		H8	−35.57	8.71	−44.3			1.06	
			CH$_3$(2)	13.62	3.13	10.5				
2,2Me$_2$Gua$^-$	9	7	H8	−28.54	7.68	−36.2				
			CH$_3$(2)	9.98	3.02	7.0				
2,2Me$_2$Gua	7		H8	−34.85	8.71	−43.6			1.21	
			CH$_3$(2)	6.03	3.13	2.9				
2,2Me$_2$Gua$^-$	7	9	H8	−66.21	7.68	−73.9			1.93	
			CH$_3$(2)	15.11	3.02	12.1				
1Me8OGuo$^-$	7		CH$_3$(1)	−1.30						
			H1′	6.80						
			H2′	7.70						
			H3′	5.60						
			H4′	5.20						
H5′	4.60									
Guo	7		H8	−27.58	8.92	−36.50	9.2	−45.7	2	13
			H1′	14.37	5.83	8.54			27	
			H2′	4.51	4.47	0.04			36	
			H3′	5.50	3.69	1.81			56	
			H4′	5.20	4.05	1.15			122	
			H5′	5.04	4.18	0.86			77	
Guo$^-$	7	1	H8	−30.37	7.76	−38.13			0.45	
			H1′	13.65	5.67	7.98			29	
			H2′	4.75	*c*				13	
			H3′	6.00	3.77	2.23			73	
			H4′	5.41	4.15	1.26			1.62	
			H5′	*c*	4.64				85	
dG	7		H8	−28.27	8.47	−36.7	9.2	−45.9	2	72
			H1′	14.50	6.26	8.2			30	
			H2′	2.48	4.55	−2.1			65	
			H2″	3.09	2.53	0.6			33	
			H3′	6.13	3.76	2.4			70	
			H4′	5.16	2.71	2.5			143	
			H5′	*c*	4.1					
dG$^-$	7	1	H8	−31.24	7.76	−39.0				
			H1′	15.32	6.18	9.1				
			H2′	2.68	4.49	−1.8				
			H2″	3.51	2.33	1.2				
			H3′	6.53	2.48	4.1				
			H4′	5.37	2.63	2.7				
			H5′	*c*	4.01					
5′GMP	7		H8	−26.05	8.13	−34.2	9.2	−43.3	2	13
			H1′	13.82	5.85	8.0			41	
			H2′	3.86	4.7	−0.8			31	
			H3′	6.90	4.43					
			H4′	5.66	4.26	1.4			121	
			H5′	6.90	3.93	3.0			51	
5′GMP	7	1	H8	−27.45	8.09	−35.5			25	
			H1′	14.40	5.85	8.6			32	
			H2′	3.91	4.69	−0.8			32	
			H3′	7.36	4.41	3.0			38	
			H4′	5.96	4.24	1.7			80	
			H5′	7.41	3.9	3.5			43	
Hyp	7		H2	4.15	8.21	−4.1	−1.3	−2.8	10.6	15
			H8	−18.28	9.01	−27.3	10.1	−37.4	2.12	
Hyp$^-$	7	9	H2	−8.59	7.92	−16.5			11.8	
			H8	−34.31	8.01	−42.3			0.71	
7MeHyp	9		H2	8.85	8.24	0.6				15
			H8	−8.10	8.99	−17.1			1.24	
			CH$_3$(7)	20.34	4.11	16.2				

Table 3 (Continued)

ligand	coord. site	ion site	proton	δ (ppm)	δ_{dia}[a] (ppm)	δ_{iso} (ppm)	δ_{dip} (ppm)	δ_{con} (ppm)	T_1[b] (ms)	synth ref
7MeHyp$^-$	9	1	H2	9.50	7.79	1.7				
			H8	−8.30	7.95	−16.3				
			CH_3(7)	32.86	3.86	29.0				
7MeHyp	3		H2	−16.35	8.24	−24.6				15
			H8	12.82	8.99	3.8			1.06	
			CH_3(7)	5.01	4.11	0.9				
7MeHyp$^-$	3	1	H2	−20.19	7.79	−28.0				
			H8	19.28	7.95	11.3				
			CH_3(7)	13.74	3.86	9.9				
Ino	7		H2	4.71	8.26	−3.6	−1.2	−2.3	45	15
			H8	−15.70	9.2	−24.9	16.5	−41.4	1.38	
			H1′	12.34	6.12	6.2			35	
			H2′	3.88	4.62	−0.7			114	
			H3′	4.90	4.3	0.6			106	
			H4′	5.07	4.19	0.9			79	
			H5′	5.18	3.8	1.4			85	
Ino$^-$	7	1	H2	*c*	8.03					
			H8	−20.22	8.05	−28.3			1.89	
			H1′	14.49	5.93	8.6			26	
			H2′	4.68	4.74	−0.1			2.38	
			H3′	4.93	4.35	0.6			52	
			H4′	5.86	4.21	1.7			10	
			H5′	6.09	3.79	2.3			66	
5′IMP	7		H2	4.59	8.12	−3.53	−1.3	−2.3		15
			H8	−14.85	8.5	−23.35	17.3	−40.6		
			H1′	11.54	6.05	5.49				
			H2′	3.24	3.95	−0.71				
			H3′	6.14	4.3	1.84				
			H4′	5.21	4.72	0.49				
			H5′	6.63	4.44	2.19				
5′IMP$^-$	7	1	H2	*c*	8.07					
			H8	−17.41	8.34	−25.75				
			H1′	12.80	5.98	6.82				
			H2′	3.55	3.91	−0.36				
			H3′	5.64	4.25	1.39				
			H4′	*c*	4.71					
			H5′	7.13	4.35	2.78				
8-O-Hyp$^-$	7	7	H2	−38.30					0.62	7
8-O-Hyp^{2-}	7	7, 9	H2	−39.95						
8-O-Hyp^{3-}	7	1, 7, 9	H2	−50.00						
8-O-Ino$^-$	7	1	H2	−36.10	7.99	−44.1			0.56	7
			H1′	7.30	5.66	1.6				
			H2′	7.70	4.83	2.9				
			H3′	5.56	4.12	1.4				
			H4′	5.24	3.84	1.4				
			H5′	4.55	3.57	1.0				
8-O-Ino^{2-}	7	1, 9	H2	−33.19						
			H1′	*d*						
			H2′	7.75						
			H3′	5.67						
			H4′	5.57						
			H5′	*c*						
1,3Me$_2$Xan	7		H8	−23.23	8.38	−31.6				14
			CH_3(1)	4.36	3.44	0.9			72	
			CH_3(3)	3.89	3.23	0.7			55	
1,3Me$_2$Xan$^-$	7	9	H8	−52.43	7.44	−59.9				
			CH_3(1)	10.60	3.37	7.2			30	
			CH_3(3)	5.37	3.21	2.2			38	
1,3,7Me$_3$Xan	8	CH_3(1)	3.60	3.31	0.3					14
trans-Cl			CH_3(3)	7.48	3.12	4.4				
			CH_3(7)	24.69	3.8	20.9			2.5	
1,3,7Me$_3$Xan$^-$	8	9	CH_3(1)	4.65						
trans-Cl			CH_3(3)	5.13						
pH 3.78			CH_3(7)	33.73						
1,3,7Me$_3$Xan	8		CH_3(1)	4.68	3.31	1.4				
trans-H$_2$O			CH_3(3)	4.32	3.12	1.2				
			CH_3(7)	62.57	3.8	58.8			0.93	
1,3,7Me$_3$Xan$^-$	8	9	CH_3(1)	4.50						
trans-H$_2$O			CH_3(3)	13.81						
			CH_3(7)	91.00						
1,3,7Me$_3$Xan$^-$	8	9	CH_3(1)	4.17						
trans-OH$^-$			CH_3(3)	12.71						
			CH_3(7)	59.69						

[a] Free ligand values. [b] Generally, values greater than ~2 ms were measured by the inversion-recovery technique. Asterisked values were estimated as $T_1 = T_2 = 1/\pi\Delta\nu_{1/2}$. [c] Obscured by HOD peak. [d] Obscured by overlapping resonance. [e] Estimated for the free ligand.

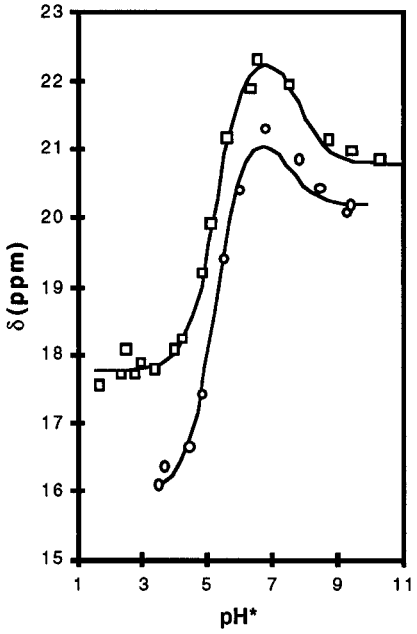

Figure 3. Plot of $\delta(^{31}P)$ versus pH for [(5′GMPκ^{N7})$(NH_3)_5Ru^{III}$] (○) and [(5′IMPκ^{N7})$(NH_3)_5Ru^{III}$] ([□]).

Table 4. ^{31}P NMR Chemical Shifts in [L$(NH_3)_5Ru^{III}$] at 19 °C in D_2O, where L = 5′GMP and 5′IMP

ligand	δ (ppm)	δ_{ligand} (ppm)	δ_{iso} (ppm)
5′GMP	16.09		
5′GMP^{2-}	20.42	5.13	15.29
5′IMP	17.71		
5-IMP^{2-}	20.97	5.27	15.70

as *trans*-[(H_2O)(1,3,7Me$_3$Xanκ^{C8})$(NH_3)_4Ru^{III}$], the corresponding N9-ionized complex, and the N9-ionized hydroxo complex.

^{31}P-NMR. Table 4 lists the ^{31}P-NMR resonances for the 5′GMP and 5′IMP complexes. Assuming the phosphate to be a monoanion in the pH 2−3 range, Ru^{III} at the N7 of these nucleotides shifts the resonance 11−13 ppm downfield relative to $H_2PO_4^-$. As the pH approaches 7, the resonance shifts an additional 3 ppm downfield. Finally, above pH 7, the signal moves back 1−2 ppm upfield. The ^{31}P-NMR signal of the 5′GMP complex is plotted as a function of pH in Figure 3. This curve was fit to the following equation:

$$\delta = \delta_1 + \frac{(\delta_2 - \delta_1)[H^+]K_{a1} + (\delta_3 - \delta_1)(K_{a1}K_{a2})}{[H^+]^2 + [H^+]K_{a1} + K_{a1}K_{a2}}$$

Here $\delta_1 = 15.84$, $\delta_2 = 21.60$, $\delta_3 = 20.20$, p$K_{a1} = 5.2$, and p$K_{a2} = 7.40$. An analogous plot for the 5′IMP complex is also shown in Figure 3, where $\delta_1 = 17.70$, $\delta_2 = 22.5$, $\delta_3 = 20.8$, p$K_{a1} = 5.2$, and p$K_{a2} = 7.8$. The first ionization (pK_{a1}) in both complexes is attributed to ionization from the phosphate, while the second one is accompanied by a color change in the $\pi-d_\pi$ LMCT range, consistent with ionization from N1 in the corresponding nucleoside complexes.[13,29]

The ^{31}P-NMR signal of sonicated calf-thymus DNA was markedly broadened by ion-pair interactions with $[(NH_3)_6Ru]^{3+}$ or coordination by $[(NH_3)_5Ru^{III}]$ or *cis*-$[(NH_3)_4Ru^{III}]$. For $[(NH_3)_6Ru]^{3+}$, precipitation occurred at $[Ru^{III}]/P_{DNA} > 0.25$, which placed an upper limit on the ruthenium concentration. Since the pentaammine complex was added to the DNA as Ru^{II}, higher reactant ruthenium(II) concentrations ($[Ru^{II}]/P_{DNA} \leq 0.75$) were possible, while for *cis*-$[(H_2O)_2(NH_3)_4Ru^{II}]^{2+}$ this ratio was limited to 0.2. The line width approximately tripled through outer-sphere interactions with $[(NH_3)_6Ru]^{3+}$ at $[Ru^{III}]/P_{DNA} >$ 0.1. Increasing the temperature from 30 to 60° decreased the line widths by half. Only slight upfield shifts (0.5−1.0 ppm) from the free DNA resonance (4.09 ppm) were evident with increasing $[(NH_3)_6Ru]^{3+}/P_{DNA}$ ratios from 0.1 to 0.25.

Measurements of ^{31}P NMR chemical shifts for $[(NH_3)_5Ru^{III}]_n$−DNA were done at 60 °C because the line widths at 30 °C were so broadened as to give unacceptable signal to noise levels. In contrast to the upfield shift observed for $[(NH_3)_6Ru^{III}]$·DNA, at 60° the ^{31}P NMR chemical shift of the $[(NH_3)_5Ru^{III}]_n$−DNA complex moved downfield only 0.07 ppm relative to the free ligand but moved upfield by 0.40 ppm as the reactant $[Ru^{II}]/P_{DNA}$ ratio increased from 0.25 to 0.75. For none of the ruthenium species was a resonance discrete from the $^{31}P_{DNA}$ envelope observed.

Relaxation Times. T_1 measurements for selected complexes are listed in Table 3. Owing to the severe broadening that precluded using the inversion-recovery method, a number of T_1's were estimated from line widths. T_1's of protons on the free ligands are generally in the range 1.0−6.0 s. Upon complexation with $[(NH_3)_5Ru^{III}]$, the T_1's of the ring protons decrease by 2−3 orders of magnitude to the range of 1−50 ms, while those for the sugar protons (notably H1′) decreased by 1−2 orders of magnitude. T_1's for the alkyl protons in the theophylline and inosine complexes decreased upon ionizing the purine ring, whereas in the guanosine complex only that for H2′ decreases significantly, while those for H3′−H5′ increase substantially. In the Guo and Ino complexes, T_1 for H8 decreases upon N1 ionization, whereas in the 5′GMP complex it increases. Due to broadening by proton exchange, all T_1's reached a minimum in the pH region around the pK_a of the complex. A correlation between T_1 and distance to the ionization site is evident for H8, H1′, and H2′.

Geometric Correlations with Paramagnetic Effects. The ^1H NMR paramagnetic isotropic shifts listed in Table 3 were estimated as the difference between the observed shift for a given proton in the complex and that for the free ligand ($\delta_{iso} = \delta_{obs} - \delta_{ligand}$). The contact (through bond) paramagnetic shift (δ_{con}) was estimated as $\delta_{con} = \delta_{iso} - \delta_{dip}$, where the dipolar (through space) pseudocontact shift (δ_{dip}) was calculated according to the methods given in the experimental section by using the EPR *g*-values of the Ru^{III} complexes listed in Table 5. The assignment of *g*-values was made according to the best fit between the resulting δ_{con} values and the signs of the calculated hyperfine coupling constants (A)[32,38] for the ring protons in the pyridine complex, which was consistent with those values calculated for the ring protons in the purine complexes. This lead to the ordering of $g_x > g_y > g_z$ for these complexes.

In solution, the various sugar conformations of nucleosides and nucleotides exist in rapid equilibrium.[43] The most common orientations for purine nucleosides (C2′-*endo*/*syn*/*gg*, C2′-*endo*/*anti*/*gg*, and C3′-*endo*/*anti*/*gg*)[44] were initially considered as dominant forms.[45] Nucleotide complexes with metal cations at N7 generally adopt an *anti* configuration that allows for ion-pairing between the metal and the phosphate. Models for the nucleotide complexes were constructed from atomic positions of a number of free nucleotides and metal−nucleotide complexes extracted from the Cambridge Structural Database.[28] Correlation values ($-R_cR_d$) between the δ_{dip} and δ_{con} values in the Guo, Ino, 5′GMP, and 5′IMP complexes and the trends in these values expected for the various crystallographically derived

(43) Saenger, W. *Principles of Nucleic Acid Structure*; Springer-Verlag: New York, 1984; p 556.
(44) Gelbin, A.; Schneider, B.; Clowney, L.; Hsieh, S.-H.; Olson, W. K.; Berman, H. M. *J. Am. Chem. Soc.* **1996**, *118*, 519−529.
(45) Viswamitra, M. A.; Seshadri, T. P. *Nature* **1974**, 176−177.

Table 5. Measured and Calculated EPR *g*-Values for [L$(NH_3)_5Ru^{III}$], Where L = Heterocyclic Ligand, Nucleosides at −130 to −140 °C in 50:50 Ethylene Glycol/Water, and Calculated Values in Parentheses[a,b]

ligands	g_1 (g_1(calc))	axes	g_2 (g_2(calc))	axes	g_3 (g_3(calc))	axes	Δ[f]	$\|V\|$	T_1[g]	T_2	T_3
Cl^- [c]	2.98 (−3.08)	*z*	1.51 (−1.58)	*y*, *z*	0.99 (1.05)	*y*, *z*	−0.92	0.16	0.69	0.61	0.38
py[d]	2.82 (2.83)	*x*	1.86 (−1.87)	*y*, *z*	(1.10)	*y*, *z*	−0.6	0.24	0.69	0.63	0.35
2MeIm[e]	2.90 (−2.90)	*z*	2.18 (2.18)	*x*	(0.51)	*y*	0.76	0.44	0.76	0.51	0.40
Ino	2.97 (2.99)	*x*	1.37 (1.40)	*y*	(1.40)	*z*	−0.75	0.0	0.64	0.64	0.41
Guo	3.01 (3.01)	*x*	1.46 (−1.49)	*y*	(1.28)	*z*	−0.78	0.07	0.66	0.63	0.40
8-O-Guo^- [h]	2.59 (−2.59)	*x*	2.35 (2.35)	*y*	1.84 (1.84)	*z*	4.8	2.0	0.99	0.14	0.09
5′IMP	2.97 (2.99)	*x*	1.37 (1.40)	*y*	(1.40)	*z*	−0.75	0.0	0.64	0.64	0.41
5′GMP	3.01 (3.01)	*x*	1.46 (−1.49)	*y*	(1.28)	*z*	−0.78	0.07	0.66	0.63	0.40

[a] The observed *g*-values are listed as positive quantities, while the calculated *g*-values are given the proper sign for the convention used. Where no measured *g*-value is given, the quantity was not observed experimentally. $T = 2$ K, except where noted. [b] Axis system:

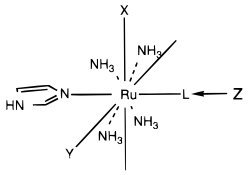

[c] Taken from refs 73−75. [d] Taken from ref 10 but axes are reassiged on the basis of NMR shift data. [e] Axes assigned on the same basis as similar imidazole complexes in ref 10. [f] Δ is the tetragonal ligand field distortion parameter, and *V* is the rhombic distortion parameter in the electron (rather than hole) formalism. [g] Ground-state coefficients for the ground state in the hole model (see Figre 1 in ref 10). [h] $T = 130-140$ K; *g* values were fit by using $k = 1.15$.

sugar conformations are summarized in Figures S10 through S13 in the Supporting Information. These correlations suggest a slight preference for *syn* conformations with guanosine as a ligand (Figure S10) but a preference for *anti* conformations with inosine (Figure S12). The corresponding nucleotide correlations exhibit a clear preference for *anti* over *syn* conformations.

Discussion

Structure. The decrease of the Ru−N9 bond distance by 0.021 Å and increase in the pK_a of N1 by 0.46 in going between [(7MeHypκ^{N9})$(NH_3)_5$Ru]$^{3+}$ [28] and [(7MeGuaκ^{N9})$(NH_3)_5$Ru]$^{3+}$ arises from the electron-donating amine at C2 of the latter, which increases electron density on the guanine ring.[29] The decrease in the pK_a of the N1 site in [(7MeGuaκ^{N9})$(NH_3)_5$Ru]$^{3+}$ by 1.60 relative to free 7MeGua[46] is close to the predicted value of 1.69 on the basis of the inverse square relationship that holds for heterocyclic complexes of pentaammineruthenium(III), $\Delta pK_a = 1.36/r^2 - 2.67$, where *r* is the distance in nm between the Ru^{III} and the nitrogen ionization site.[29]

Autoxidation Kinetics. As oxygen is required for the oxidation of [L$(NH_3)_5Ru^{III}$], where L = guanine or hypoxanthine[7] derivatives, the reactions described here are, indeed, autoxidation reactions, as opposed to another hydroxide-induced oxidations of aromatic rings on Ru^{III}.[47] While the suggested mechanism for the autoxidation of purine nucleosides induced by the presence of the $(NH_3)_5Ru^{III}$ was predicated upon an initial H8 ionization,[7] the data are also consistent with an initial nucleophilic addition of the hydroxide at C8 as shown in Figure 4, which is more in line with the relatively small isotope effect ($k_H/k_D = 1.6$) observed in the inosine study.[7] On the basis of k_{obs} under the same conditions (pH 11, $[O_2] = 0.269$ mM), the autoxidation of the Guo complex proceeds ∼5 times slower than that for the Ino complex. This is attributed to a slightly higher electron density at C8, which arises from the electron-donating exocyclic amine. Increased negative charge slows the initiating step by making C8 less susceptible to hydroxide attack (or by decreasing the ionization constant for H8 deprotonation). In keeping with this, the rates are significantly slower for the Guo and dGuo ligands, which ionize at N1 and thereby enhance negative charge at C8, as opposed to the 1MeGuo case, which cannot ionize at N1.

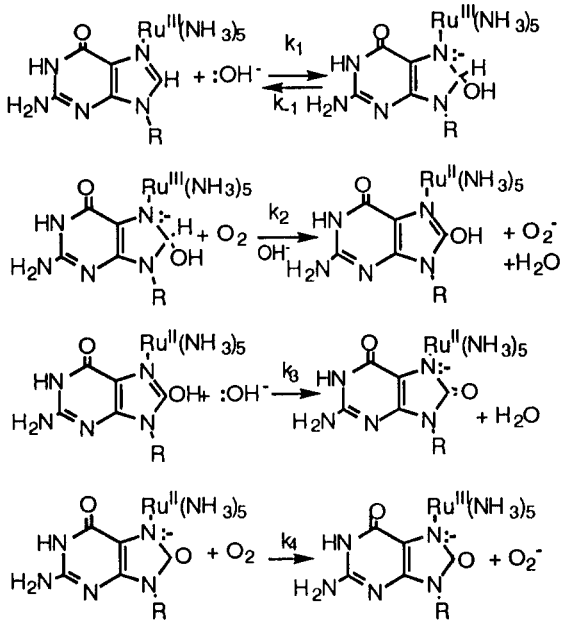

Figure 4. Possible mechanism for the autoxidation of [(Guoκ^{N7})$(NH_3)_5$-Ru^{III}].

Magnetic Resonance Spectroscopy. Previous EPR studies on complexes of the type *trans*-[L(Im)$(NH_3)_4Ru^{III}$] showed that these complexes generally exhibit rhombic EPR spectra with g_3 being unobservable (<1.0) in conventional EPR spectrometers. In the imidazole complexes, the relative participation of d_{xz} and d_{yz} in the ground state varies inversely depending on the π-donor characteristics of L.[10,11] Consequently, assignments of the magnetic axes are inverted for the π-acceptor pyridine complexes relative to the π-donor imidazole complexes.[11] Involvement of lower lying π*-orbitals may account for the ordering of the *g* values for the purine complexes being more in line with the pyridine rather than the imidazole species. Table 5 lists the calculated ground-state coefficients for the d orbitals in the hole model.

The $^2T_{2g}$ ground states of both Ru^{III} and Fe^{III} generate short electronic relaxation times ($T_{1e} \sim 10^{-11}$ s) and relatively long

(46) Dawson, R. M. C.; Elliott, D. C.; Elliott, W. H.; Jones, K. M. *Data for Biochemical Research*, 2nd ed.; Oxford University Press: Oxford, U. K., 1969; p 158.
(47) Ghosh, P. K.; Brunschwig, B. S.; Chou, M.; Creutz, C.; Sutin, N. *J. Am. Chem. Soc.* **1984**, *106*, 4772−4783.

nuclear relaxation times ($T_1 \simeq 10^{-2}-10^{-4}$ s), which give well-resolved ^{1}H NMR spectra[48] but generally obscure proton−proton coupling. INDO calculations for *trans*-$(Im)_2Fe^{III}$−porphyrin[49,50] and *trans*-$[L(Im)(NH_3)_4Ru^{III}]$ systems[10] indicate that ligand-to-metal π-charge transfer accounts for spin transfer into the highest bonding orbital of the axial imidazoles. This is consistent with the LMCT bands that are prominent in the ultraviolet absorption spectra of the pyridine,[51] imidazole,[17] and purine[29] complexes of $[(NH_3)_5Ru^{III}]$, which are indicative of $\pi-d_\pi$ interactions.

In contrast with polypyridyl complexes of Fe^{III}, which exhibit larger σ-spin delocalization, polypyridyl complexes of Ru^{III} show significantly greater π-spin density delocalization, which arises from the larger extension of 4d relative to 3d orbitals.[52] Consequently, Fe^{III} and Ru^{III} differ appreciably in their paramagnetic effects on heterocyclic protons.[34]

Pyridine Complexes. The alternating signs of the δ_{iso}'s and δ_{con}'s between adjacent ring protons in the ^{1}H NMR of the pyridine complexes (cf. Table 3) and the opposite signs between δ_{iso}'s for the ring protons and the methyl resonances at the same site are consistent with π-spin density delocalization (as in simple Hückel calculations of the benzyl radical).[53] The large negative δ_{iso}'s and δ_{con}'s of the H2 and H4 protons indicate substantial negative spin (↓) density at these sites,[54] which results from the transfer of the positive spin (↑) of the unpaired metal electron through the π-HOMO with concomitant polarization of the reverse spin on the ring hydrogens.[33,55] The much smaller δ_{iso} (and positive δ_{con}) of H3 is in keeping with a node or near node at the *meta* position with the opposite spin density resulting from spin polarization from the adjacent carbons.[55,56] The somewhat larger value of δ_{iso} for H2 over H4 is consistent with an attenuated σ contribution and a negative dipolar contribution at the more distant site.[54] For analogous reasons, the line widths of the *ortho* and *para* resonances are approximately 1 order of magnitude larger than the *meta* protons (H2 > H4 ≫ H3). The slight increases in δ_{iso} of the remaining ring protons caused by methyl substitution can be attributed to increased electron density in the ring resulting in an increase of ligand to metal charge transfer and consequent increase in spin density on the ring. The slightly larger shift ($|\delta_{iso}|$, cf. Table 3) of the methyl protons at the *para* position relative to that of the corresponding ring proton can be attributed to increased electron density on the nitrogen arising from a resonance in which the methyl group contributes to the π-system.[55]

The pseudocontact shifts in the pyridine complexes are sufficiently large to be of help in ascertaining the binding of these complexes to proteins and thereby assist in determining their mode of action in anticancer or anti-T cell therapies For example in $[(py)(NH_3)_5Ru^{III}]$ at 7 Å, δ_{dip} ranges from −0.54 to 6.3 ppm. This, coupled with the high anisotropy and magnetic relaxation effects should make it possible to map the binding geometry with nonrotating Ru^{III} pyridine complexes.

C-Bound Xanthine. For both *trans*-$[X(1,3,7,Me_3Xan\kappa^{C8})(NH_3)_4Ru^{III}]$, where X = Cl^-, H_2O, and OH^-, and the corresponding κ^{C2}-bound imidazole series of complexes,[11] an inverse relationship exists between the π-donating properties of the ligand *trans* to the ylidene and the paramagnetic shifts of the methyl on the imidazole ring, $\delta(CH_3(7))$. The formation of a stronger π-bond to the anionic *trans* ligands decreases the amount of π-bonding spin density transferred onto the nitrogen heterocycle so that $\delta(CH_3(7))$ is smaller. Similarly, increasing π-donation of the xanthine ligand by ionization at N9 increases spin transfer and enhances $\delta(CH_3(7))$.

N7-Bound Purines. The H8 resonances in the κ^{N7} complexes of the purine ligands, as in the corresponding H2 of $[(Im)(NH_3)_5Ru^{III}]$,[10,11] exhibit large upfield chemical shifts and very broad line widths. For both the guanine and hypoxanthine ligands, δ_{iso} for H8 (and δ_{iso}(H2) in the hypoxanthine series) varies with the size of the N9 substituent as H ≫ CH_3 > deoxyribose > ribose > ribose monophosphate in both the neutral and ionized complexes. This is probably due to increased amounts of spin density being transferred from the ring onto the N9 substituent as the polarizability of the N9 substituent increases with size.

The larger δ_{iso}(H8) in the guanine relative to the hypoxanthine series of complexes arises from the π-donor C2-amine-enhancing Gua−Ru, $\pi-d_\pi$ bonding, which increases the spin density transferred into the purine. This type of bonding is also increased upon ionization so that ionizing $[(Hyp\kappa^{N7})(NH_3)_5Ru]^{3+}$ at N9 shifts the δ_{iso}'s for both H2 and H8 further upfield. While N1 ionization in the Ino and 5′IMP complexes also causes δ_{iso}(H8) to move upfield, that for H2 moves downfield, which probably reflects different charge distributions in N1 versus N9 ionizations. Similarly, in the methylguanine complexes a relatively larger chemical shift is exhibited by CH_3(9) compared to CH_3(2) upon ionization at N1.

The methyl groups on N1 and N3 of theophylline ($1,3Me_2$-Xan) show small downfield shifts indicative of the transfer of spin density through the π system of the ring and consistent with alternation in the spin density between adjacent positions in the aromatic ring. The H2 resonances in the 8-oxohypoxanthine and the 8-oxoinosine complexes are shifted substantially more upfield than in the κ^{N7}-bound Hyp and Ino complexes, indicating that the hypoxanthine spin density pattern is retained, but spin transfer is increased owing to the anionic character of the ligand. The upfield shift in the methyl resonance of $[(8\text{-}O\text{-}1MeGuo)(NH_3)_5Ru^{III}]$ suggests negative spin density at N1 in the guanosine complexes.

N3- and N9-Coordinated Complexes. Similar to the N7-bound complexes of guanine ligands, N9-coordination of $1,7Me_2$Gua, 7MeGua, and $N_2N_2Me_2$Gua results in upfield shifts for H8, so that the magnitude varies inversely with the size of the N7 substituent (H ≫ CH_3). However, ionization at N1 results in a smaller downfield shift relative to the N7 bound complexes, which provides a basis for distinguishing between the N9- and N7-bound complexes of $N_2N_2Me_2$Gua.

The pattern of chemical shifts in $[(7MeHyp\kappa^{N9})(NH_3)_5Ru^{III}]$ also exhibits δ_{iso}(H8) substantially upfield in the neutral-ligand complex but decreases slightly upon ionization from N1. On the other hand, metal coordination at N9 alters the spin density pattern in the pyrimidine ring by placing negative spin density on C2 thereby shifting δ_{iso}(H2) slightly downfield, which is opposite δ_{iso}(H2) in $[(Hyp\kappa^{N7})(NH_3)_5Ru^{III}]$. Coordination at N3 in $[(7MeHyp\kappa^{N3})(NH_3)_5Ru]^{3+}$ results in a substantial upfield shift in δ(H2), which exhibits greater line broadening than H8 due to H2′'s proximity to the metal ion. Moreover, this is the only complex in which H8 exhibits a downfield shift, which suggests negative spin density at C8 and readily distinguishes between the N3 and N7 or N9 isomers.

(48) Jesson, J. P. In *NMR of Paramagnetic Molecules*; La Mar, G. N., Horrocks, W. D., Holm, R. H., Eds.; Academic Press: New York, London, 1973; pp 2−51.
(49) Satterlee, J. D.; La Mar, G. N *J. Am. Chem. Soc.* **1976**, *98*, 2804−2808.
(50) Chacko, V. P.; La Mar, G. N. *J. Am. Chem. Soc.* **1982**, *104*, 7001−7007.
(51) Curtis, J. C.; Meyer, T. J. *Inorg. Chem.* **1982**, *21*, 1563.
(52) Desimone, R. E.; Drago, R. S. *J. Am. Chem. Soc.* **1970**, *92*, 2343−2352.
(53) Roberts, J. D. *Molecular Orbital Calculations*; W. A. Benjamin, Inc.: New York, 1962.
(54) La Mar, G. N. In *NMR of Paramagnetic Molecules*; La Mar, G. N., Horrocks, W. D., Holm, R. H., Eds.; Academic Press: New York, London, 1973; pp 86−123.
(55) Drago, R. S. *Physical Methods for Chemistry*, 2nd ed.; Saunders College Publishing: Ft. Worth, TX, 1992.
(56) Eaton, D. R.; Josey, A. O.; Philips, W. D.; Benson, R. E. *J. Chem. Phys.* **1962**, *17*, 347−360.

Glycosidic Protons. The paramagnetism of the metal ion presents difficulties in measuring coupling constants and nuclear Overhauser effects,[57,58] so that these are of minimal use in establishing sugar conformations in complexes of Ru^{III}. Previous studies have indicated that the sugar conformation in N7-coordinated nucleosides is relatively unaffected by monofunctional metal binding.[36,43,59] On the other hand, in metal complexes of N7-coordinated nucleotides, such as [5′IMP-$(H_2O)_5$Ni,[60] *cis*-[(5′IMP)$_2(NH_3)_2Pt^{II}$,[61] [5′IMP$(H_2O)_5Co^{II}$],[62] and 5′GMP complexes of *cis*-$[(NH_3)_2Pt]^{2+}$,[63] the phosphate generally interacts directly or indirectly through a water molecule with the hydrogen-bonding ligands on the metal ion resulting in an *anti*,*gg* sugar conformation.

The distinct change in the patterns of the sugar resonances for [5′GMP$\kappa^{N7}(NH_3)_5Ru]^{3+}$ and [5′IMP$\kappa^{N7}(NH_3)_5Ru]^{3+}$ relative to those of the corresponding nucleoside complexes, such that δ_{iso}(H5′) is significantly larger and becomes second in magnitude only to δ_{iso}(H1′), indicate that electrostatic and hydrogen bonding interactions between the phosphate and the $[(NH_3)_5Ru]^{3+}$ brings this phosphate end of the ribose closer to the paramagnetic center. Similarly, the nucleotide complexes exhibit distinctly higher correlations for *anti* forms (Supporting Figures S3−S6), which allow for electrostatic and hydrogen bonding interactions between the metal ion and phosphate.[36]

The large ^{31}P NMR chemical shifts (cf. Table 4) in the nucleotide complexes, which suggests a substantial change in P−O torsion angles, and the increase in acidity of the phosphate ($\Delta pK_a = 0.8$) are also consistent with such phosphate−Ru^{III} outer-sphere interactions.[64] Decreases in T_1 between H1′ and H2′ and between H4′ and H5′ for the 5′GMP relative to the Guo complex are also in harmony with *anti*,*gg* conformations in which H2′ is generally closer to the metal ion than H1′ and the electrostatic interaction between the metal and the phosphate similarly brings H5′ closer to the metal than H4′. Consequently, the significant differences evident in Table 3 between the guanosine and inosine complexes probably lie in different populations of the orientations about the glycosidic bond possibly arising from [(Guoκ^{N7})$(NH_3)_5Ru^{III}$] existing in solution with little discrimination between *syn* and *anti* components,[45,65,66] while the analogous inosine complex retains more of an *anti* conformation.[67]

In both the guanosine and the 8-oxo complexes, in which the oxygen is expected to exert a steric effect inducing a higher *syn* component,[43,68] the relative shifts follow the ordering H3′ > H4′ > H5′, whereas the ordering is H5′ > H4′ > H3′ for the inosine complex. The similarity of patterns for the sugar resonances for the nucleotide and inosine complexes (H1′ ≫ H5′ > H4′ ∼ H3′ > H2′) is consistent with a heavily *anti* glycosidic orientation for both. The alteration in the relative shifts of H1′ and H2′ generated by the presence of the 8-oxo group such that H2′ > H1′ may arise from increased spin density delocalized into the sugar ring in the 8-oxo complexes whereby the anionic ligand can better π-bond to the metal. Alternatively, increased spin density on the ring may enhance the expected upfield shift for H1′ and downfield shift for H2′ due to N3 electron pair magnetic anisotropy[57] for C2′-*endo* sugars in the *syn* conformation.

While the energy barrier for the *syn*/*anti* interconversion is low (-1 kcal/mol) for both purine nucleosides resulting in rapid equilibria,[69] MO calculations indicate that guanosine prefers the *syn* over the *anti* conformation while inosine tends to prefer the *anti*.[57] With the exception that δ_{iso}(H4′) > δ_{iso}(H3′), the sugar resonance pattern and the magnitudes of δ_{iso}'s are similar for the deoxyguanosine and guanosine complexes, suggesting that the dG complex also exhibits a relative preference for the *syn* conformation. Also, X-ray crystallographic studies and MO calculations show that the *syn* orientation in dG can be stabilized by hydrogen bonding between O5′-H and N3.[43,70] Overall, it is likely that Ru(III) κ^{N7}-complexes of guanine nucleosides have a higher *syn* component than the corresponding inosine and nucleotide complexes.

Conclusions. In complexes of the type $[L(NH_3)_5Ru^{III}]$, the following holds:

(1) Paramagnetic shifts in the aromatic protons of purine bases can be used to distinguish between N3, N7, and N9 linkage isomers, with δ_{iso} for H8 being strongly upfield (∼−30 ppm) for N7, less so for N9 (∼−17 ppm), and downfield for N3 (∼4 ppm). Of course, in 8-coordinated complexes this resonance is absent.

(2) The sugar resonances yield very different NMR resonance patterns, depending upon the configuration of the sugar. Despite the paramagnetic effects that preclude observation of coupling in the 1D spectra, 2D COSY spectra can be obtained for sugar protons in nucleoside and nucleotide complexes and can be used to assign these resonances.

(3) ^{31}P-NMR spectra are useful for determining metal−phosphate interactions in nucleotide complexes, and shifts in δ(P) upon complexation of Ru^{III} at N7 indicate an ion-pairing/hydrogen-bonding between the metal center and the phosphate; however discrete resonances are not evident in $[(NH_3)_5Ru^{III}]_n$−DNA.

(4) EPR and ^{1}H NMR spectra should be useful in determining the binding modes of Ru^{III} immunosuppressant complexes such as [(4Mepy)$(NH_3)_5Ru^{III}$] (PRO 2844).

Acknowledgment. This work was supported by PHS Grant GM26390. We are grateful to Prof. Hans Van Willigen (Univ. of Massachusetts, Boston), who generously provided the preliminary EPR spectra, and the research group of Prof. Wilma Olson (Rutgers U.) for preprints of their work and their initial search of the CSD.

Supporting Information Available: COSY spectra, correlation plots, and complete crystallographic tables for [(7MeGua)$(NH_3)_5$Ru]-Cl_3·$3H_2O$ (31 pages). Ordering information is given on any current masthead page.

IC9609416

(57) Davies, D. *Prog. NMR Spectrosc.* **1978**, *12*, 135−225.
(58) de Ropp, J. S.; La Mar, G. N. *J. Am. Chem. Soc.* **1991**, *113*, 4348−4350.
(59) Begum, N. S.; Poorjary, M. D.; Manohar, H. *J. Chem. Soc., Dalton Trans.* **1988**, 1303−1307.
(60) Clark, G. R.; Orbell, J. D. *Chem. Commun.* **1974**, 139.
(61) Goodgame, D. M. L.; Jeeves, I.; Phillips, F. L.; Skapski, A. C. *Biochim. Biophys. Acta* **1975**, *4022*, 153.
(62) De Meester, P.; Goodgame, D. M. L.; Jones, T. J.; Skapski, A. C. *C. R. Acad. Sci., Ser. C* **1974**, 667.
(63) Reily, M. D.; G., M. L. *J. Am. Chem. Soc.* **1986**, *108*, 8299−8300.
(64) Gorenstein, D. G.; Goldfield, E. M. In *Phosphorus-31 NMR*; Gorenstein, D. G., Ed.; Academic Press: Orlando, FL, 1984; pp 1−33, 34−51, 315.
(65) Young, D. W.; Tollin, P.; Wilson, H. R. *Acta Crystallogr.* **1974**, *B30*, 2012−2018.
(66) Young, D. W.; Tollin, P.; Wilson, H. R. *Nature* **1974**, 513−514.
(67) Thewalt, V.; Bugg, C. E.; Marsh, R. E. *Acta Crystallogr.* **1970**, *B26*, 1089−1100.
(68) Schweizer, M. P. In *Magnetic Resonance in Biology*; Cohen, J. S., Ed.; John Wiley and Sons: New York, 1980; Vol. 1, pp 259−273.
(69) Jordan, F.; Pullman, B. *Theoret. Chim. Acta (Berl.)* **1968**, *9*, 242−252.
(70) Haschemeyer, S. E. V.; Sobell, H. M. *Acta. Crystallogr.* **1965**, *19*, 125.
(71) Stanbury, D. M.; Haas, O.; Taube, H. *Inorg. Chem.* **1980**, *19*, 518−524.
(72) Clarke, M. J. *J. Am. Chem. Soc.* **1978**, *100*, 5068−5075.
(73) Carlin, R. L.; Burriel, R.; Seddon, K. R.; Crisp, R. I. *Inorg. Chem.* **1982**, *21*, 4337−8.
(74) Sakaki, S.; Hagiwara, N.; Yanase, Y.; Ohyoshi, A. *J. Phys. Chem.* **1978**, *82*, 1917−1920.
(75) Kaplan; Navon, G. *J. Phys. Chem.* **1974**, *78*, 700.